
High Responsivity Ultraviolet Photoconductors Based on Epitaxial ZnO Thin Films

Ahmed Mohammed Nahhas

Department of Electrical Engineering, Faculty of Engineering and Islamic Architecture, Umm Al Qura University, Makkah, Saudi Arabia

Email address:

amnahhas@uqu.du.sa

To cite this article:

Ahmed Mohammed Nahhas. High Responsivity Ultraviolet Photoconductors Based on Epitaxial ZnO Thin Films. *American Journal of Nano Research and Applications*. Special Issue: *Recent Advances of Nanomaterials and Devices*. Vol. 7, No. 1, 2019, pp. 6-10.

doi: 10.11648/j.nano.20190701.12

Received: July 19, 2019; **Accepted:** July 31, 2019; **Published:** September 2, 2019

Abstract: In this paper, ultraviolet (UV) detection properties of epitaxial ZnO films grown on sapphire substrates with radio-frequency magnetron sputtering is reported. The responsivity (R) of the ZnO photoconductors measured at 325 nm wavelength shows a strong dependence on the incident power (P), i.e., $R \propto P^k$ ($k = 0.7$). A responsivity of 3500 A/W (or a gain of 6000) is obtained at the optical power density of 10^{-7} W/cm², and the value decreases to 1 A/W at 10^{-2} W/cm². The ultra-high responsivity at the low power regime suggests a long lifetime (order of 10 μ s) of carriers. The enhanced carrier lifetime is explained by the preferential capture of holes at the recombination centers that exist in the depletion region around grain boundaries and film surface, and the subsequent separation of photogenerated carriers. The strong dependence of the responsivity on the incident power is attributed to the modulation of space charge region width by the photogenerated holes and the resulting change in carrier lifetime.

Keywords: ZnO, High Responsivity, Epitaxial, UV, Photoconductor, GaN

1. Introduction

ZnO possesses many interesting properties and has been extensively studied for various applications such as varistors [1], transducers [2], transparent conducting electrodes [3], sensors [4], and catalysts [5]. Being wide bandgap semiconductor, single-crystalline ZnO films and related heterostructures have recently been drawing strong attention for their potential applications in light emitting or detecting devices in the ultraviolet (UV) range [5, 6]. ZnO is isomorphic to wurtzite GaN with good lattice match, and therefore has also been used as a buffer layer in growing high quality GaN films (or vice versa ZnO growth on GaN) [7, 8]. Despite the isomorphic nature of the crystal structure, ZnO displays some of its physical properties significantly different from those of GaN. For example, ZnO shows a much larger exciton binding energy than GaN [9], and the resistivity can be relatively easily changed in a broad range by controlling the non-stoichiometric defects [10]. On the other hand, the ZnO's material properties potentially offer a unique device application, the research and the development of optoelectronic devices based on epitaxial ZnO films, in

general, has been limited comparing with the GaN case. This is mainly due to the difficulty in achieving *p*-type doping and in obtaining good quality Schottky contacts on ZnO, and also to the rather complex behavior of the material involving film surface and grain boundaries [10].

The UV photoconductors based on epitaxial ZnO films have been reported to show high responsivities, i.e., 400 A/W with ZnO films grown by metal organic chemical vapor deposition (MOCVD) or 1200 A/W with MgZnO films grown with pulsed laser deposition [11]. The responsivity (and the gain) of a photoconductor is basically determined by the ratio of the carrier lifetime to the transit time, and is, in general, known to depend on the incident power level. The dependence of the responsivity on the incident power is an important information not only for device operation but also for materials study, since it usually reflects the gain mechanisms involved, i.e., carrier trapping and recombination at the defects such as surface/interface states at the film surface and grain boundaries. In the case of epitaxial GaN films, the UV detection properties of photoconductors have been extensively studied and the gain mechanisms have been reasonably well understood [12]. In the case of epitaxial ZnO films, however,

the reports are rare that dealt with the power dependence of responsivity and the gain mechanisms responsible for the high responsivities observed. In this letter, the ultraviolet detection properties of epitaxial ZnO films grown by rf magnetron sputtering is reported. Ultra-high responsivity of 3000 A/W is obtained with the ZnO photoconductors. The power dependence of the responsivity was characterized over five decades of incident power, and the result is explained with a gain mechanism that involves interactions of photogenerated carriers with the recombination centers at grain boundaries and film surface.

2. Experimental Work and Results

The ZnO epitaxial films used in this study were grown on Al₂O₃ substrates using RF sputtering. A 5N-purity ZnO target was used in conjunction with Ar or Ar/O₂ gas as an ambient gas for sputtering. The films were deposited at 700°C in Argon gas ambient. Figure 1 shows the X-ray diffraction (XRD) analysis of the ZnO film. The results show that the films are highly epitaxial with (0001) orientation as shown. Both the electrical properties of the ZnO films and the contact properties of aluminum on ZnO were characterized with a transfer length measurement (TLM) method. 150-nm-thick Al electrodes were deposited on ZnO using thermal evaporation in conjunction with a liftoff process. Aluminum source was used for the evaporation process. In order to investigate the effect of annealing on film and contact properties, some samples were further processed with an annealing at 800°C in oxygen ambient for 30 min prior to the contact metallization [14, 15].

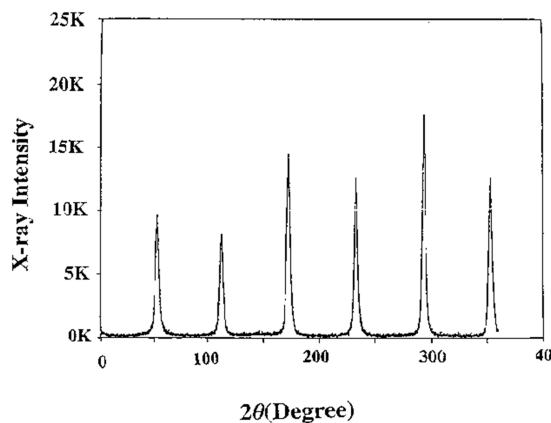


Figure 1. X-ray diffraction analysis $\theta/2\theta$ scan profile of ZnO film grown on a sapphire [14, 15].

Figure 2 shows the current-versus-voltage (I-V) characteristic of an as-deposited sample. It shows a linear behavior indicating the ohmic nature of the Al contact on ZnO. Figure 3 shows the resistance values measured as a function of inter-electrode spacing. The external voltage applied across two electrodes can be divided into two components: 1) the voltage drop that appears across the ZnO spacing region in between the two electrodes and 2) the voltage drops in the contact region. From the slope of the I-V curve, the resistivity of our ZnO film (3 μm thick) is

calculated to be 200 k Ω -cm. Assuming the electron mobility of 10 cm²/V-sec, the carrier concentration is estimated to be 3 $\times 10^{12}$ cm⁻³. The contact resistance (R_c) is read to be 1 M Ω from the y-intercept, and the transfer length (L_T) of 1 μm from the x-intercept. The specific contact resistivity (ρ_c) is then calculated to be 5 Ω -cm² using the relationship of $\rho_c = R_c W L_T$, where contact width W of 500 μm was used in this TLM work. This contact resistivity value is considered very large, at least three or four orders of magnitude higher than those that can be obtained with other semiconductors such as Si, GaAs and GaN. It is interesting to note that the Al contact on ZnO shows an ohmic character despite the relatively large value of the specific contact resistivity. With the help of figure 3 it can be shown that the amount of the voltage drop in the contact region would be equal to the drop across the spacing region of a film if the electrode spacing is designed to be equal to the transfer length. In the case that the electrode spacing is 10-20 μm and the transfer length is 1 μm , the voltage drop in the contact region would account for 5-10% of the external voltage applied [14, 15].

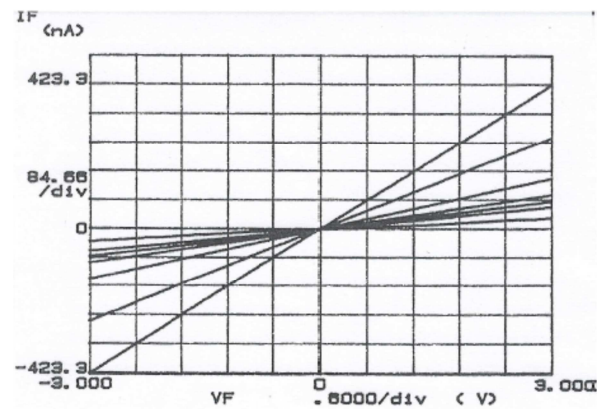


Figure 2. I-V characteristic of an as-deposited ZnO film [14, 15].

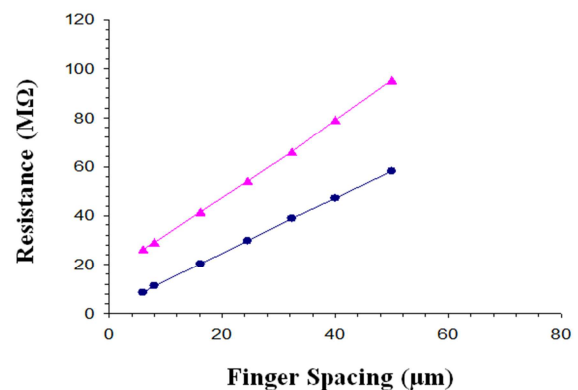


Figure 3. Resistance values measured at different electrode spacing [14, 15].

Figure 4 shows the I-V characteristics of a sample that was annealed at 800°C in oxygen ambient for 30 min prior to the aluminum metallization [14, 15]. It shows an ohmic behavior similar to the unannealed sample case. Figure 5 shows the resistance values measured at different electrode spacing. The ZnO film resistivity is calculated to be 400 k Ω -cm. The contact resistance and the transfer length are read to be 8 M Ω

and 6 μm , respectively, which correspond to the specific contact resistivity of $240 \Omega\text{-cm}^2$. It is interesting to note that the contact resistance value increased 50 times after the annealing whereas the film resistivity increased only slightly (2 times). This suggests that the oxygen annealing affected mostly the film surface properties not the film bulk. The result may be explained with the following phenomenon that might have occurred on ZnO surface with the annealing process: The annealing in oxygen ambient might have increased oxygen concentration (i.e., coverage) on the ZnO surface. Considering the fact that formation of alumina is thermodynamically favored over ZnO formation (i.e., $\Delta H_{\text{Al}_2\text{O}_3} = -1675.7 \text{ kJ/mol}$ versus $\Delta H_{\text{ZnO}} = -350.5 \text{ kJ/mol}$), the increased oxygen concentration at the Al/ZnO interface might have enhanced oxidation of Al. Formation of a thin insulating oxide layer in between Al and ZnO is then expected to increase the contact resistance. The oxygen annealing might also have altered the nature of surface states of ZnO in terms of their density and energy distributions, causing a change in the amount of Fermi level pinning and band bending and therefore the contact resistance. This surface phenomenon is expected to depend on the polarity of ZnO surface [14, 15]. Detailed mechanism, however, is not known and is a subject of further study.

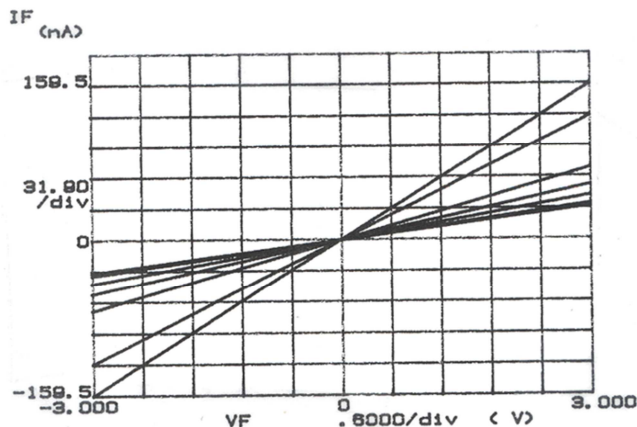


Figure 4. I-V characteristics of a sample that was annealed at 800°C [14, 15].

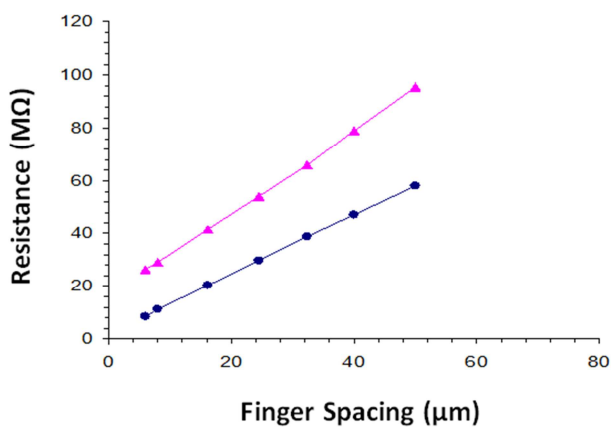


Figure 5. Resistance values measured at different electrode spacing ▲ Resistance for annealed ZnO films and ● Resistance for as-deposited ZnO films [14, 15].

For UV detection experiment with a top (vertical)

illumination configuration, the interdigitated aluminum electrodes (150 nm thick) were formed on both the as-grown and annealed ZnO samples. The electrodes were designed to have finger spacing of 10 to 20 μm , finger width of 10 μm , and finger length of 100 μm . The total area of the inter-electrode spacing is $2.5 \times 10^4 \mu\text{m}^2$. A 10-mW He-Cd laser (325 nm wavelength) was used as a UV source. The optical power density was varied in a broad range using an attenuator and also by expanding the beam. The incident power density was measured using a calibrated Si UV detector [14, 15].

Figure 6 and figure 7 show the photocurrent-versus-voltage characteristic of an unannealed sample measured at the illumination power level of $1 \times 10^{-2} \text{ W/cm}^2$ and $1 \times 10^{-5} \text{ W/cm}^2$, respectively. The dark current is also shown in figure 8. All the photo and dark currents show linear dependence on the applied voltage, indicating that the Al contact on ZnO maintains an ohmic nature independent of the carrier modulation. The photocurrent is read to be 28 mA and 2 mA at 3 V with the power density of $1 \times 10^{-2} \text{ W/cm}^2$ and $1 \times 10^{-5} \text{ W/cm}^2$, respectively, while the dark current is read 1 μA at the same voltage. This corresponds to the ON/OFF ratio of 2,000 to 28,000 in this power range. The responsivity R , defined as the ratio of the photocurrent over the optical power incident to detector surface, was calculated from the photocurrent measurement results. Figure 9 shows the responsivity measured as a function of the incident power density [14, 15]. The ZnO photoconductor shows the responsivity as high as 500 A/W measured at $1 \times 10^{-5} \text{ W/cm}^2$. The photoconductor gain (G) values are also shown in the same figure. The gain is calculated from the responsivity value using the following relationship, $G = R h\nu / \eta q$, where h is the Planck constant, ν is the frequency of the UV beam ($\lambda=325 \text{ nm}$), q is the electron charge, and η is the quantum efficiency. $\eta = 1$ is assumed in this work. The gain of 20 to 2000 is obtained from the ZnO photoconductor. The responsivity (and the gain) shows strong dependence on the incident power, $R \propto P^k$ with $k = 0.7$ [14, 15].

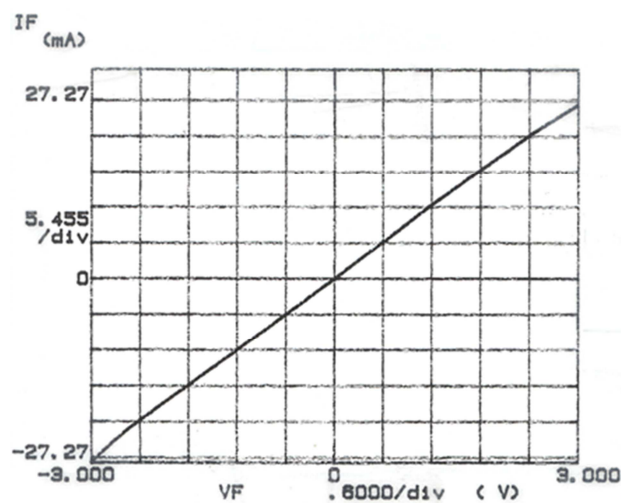


Figure 6. Photocurrent-versus-voltage characteristic of an unannealed sample with UV photoresponse at $1 \times 10^{-2} \text{ W/cm}^2$ [14, 15].

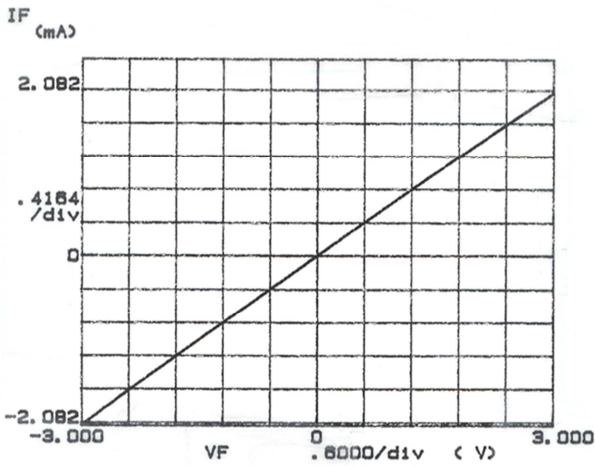


Figure 7. Photocurrent-versus-voltage characteristic of an unannealed sample with UV photoresponse at $5 \times 10^5 \text{ W/cm}^2$ [14, 15].

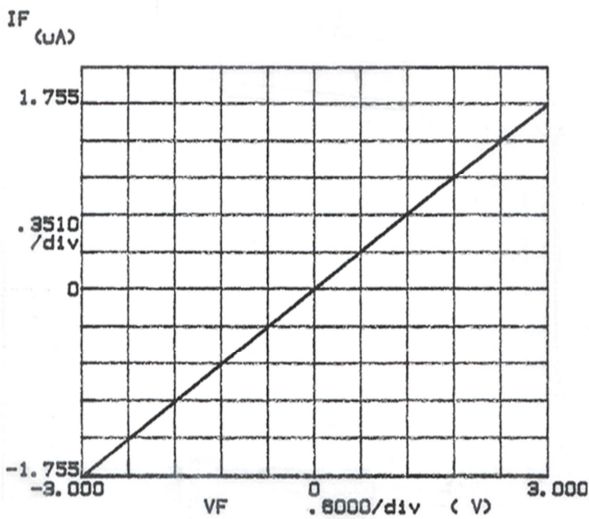


Figure 8. Photocurrent-versus-voltage characteristic of an unannealed sample for Dark current [14, 15].

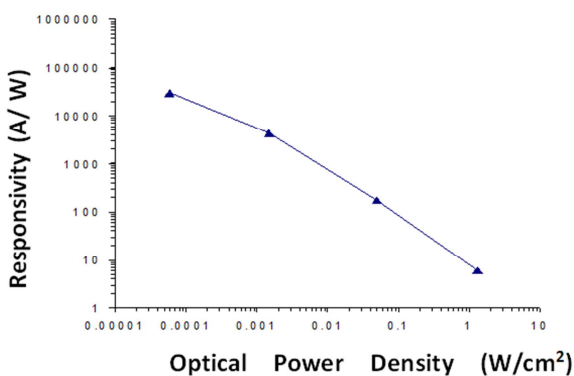


Figure 9. Responsivity vs. Optical Power Density [14, 15].

It is important to mention that a similar behavior of the power dependence of responsivity of $R \propto P^k$ ($k = 0.9$), has been reported with GaN photoconductors [14, 15]. Figure 10 shows the gain (and the responsivity) shows two orders of magnitude change (from 2000 to 20) as the power level increased three orders of magnitude [14, 15]. Assuming that

the conductive volume modulation is much less than the carrier modulation and also that no change in the donor concentration, the carrier mobility (and therefore the carrier transit time) is expected to maintain nearly the same level under different illumination power [14, 15]. This power dependence of gain (and the responsivity) observed in this work then suggests a strong dependence of the effective carrier lifetime on the illumination power [14, 15].

The undoped ZnO usually shows *n*-type conductivity mainly ascribed to the non-stoichiometric defects such as oxygen vacancies and/or Zn interstitials [13]. Considering the surface states on film surface and the resulting Fermi level pinning effect, a space charge region would form near the film surface and therefore a band bending occurs. Under UV illumination, the photocarriers are generated and the holes are swept to the depletion (i.e., space charge) region and captured by the surface states. This results in the reduction of space charge region width. The amount of this modulation would depend on the background carrier concentration and the illumination power. As discussed above, the modulation of charge region width itself is expected to be relatively insignificant compared with the carrier modulation effect in the ZnO photoconductors studied in this work [14, 15]. However, the carrier modulation would cause a certain amount of band bending change. In the dark, two opposite electron fluxes exist over the barrier, namely the thermionic emission from the metal (i.e., the aluminum electrode) towards the *n*-type ZnO and a compensating flux from the ZnO towards the metal. Under constant illumination, the photogenerated carriers reduce the band bending by V_{ph} , and this allows an electron flux to reach the surface equal to the holes arriving by drift and equal to the photocarriers generated [14, 15]. Figure 10 shows the gain-versus-power curves calculated with various different barrier heights. In this calculation the transit time of 10 ns is used assuming an electron mobility of $10 \text{ cm}^2/\text{V-sec}$ and $l = 20 \mu\text{m}$ and $V = 3 \text{ V}$. The Richardson constant $A = 110$ was assumed in this calculation. The calculation $\Delta\psi_o = 0.8 \text{ eV}$ shows a best fit with the measurement result [14, 15]. The gain curve shows a power dependence of $P^{-0.8}$ [14, 15].

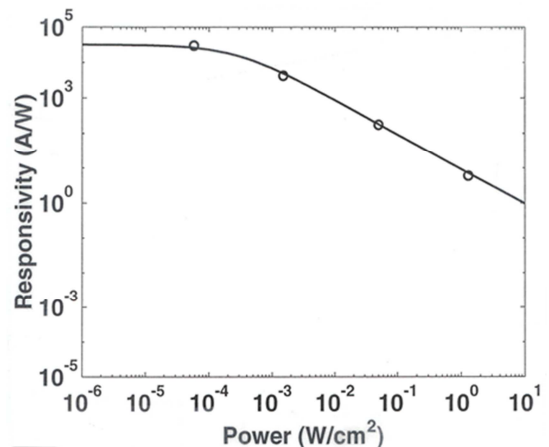


Figure 10. Gain-versus-power curves calculated with various different barrier heights [14, 15].

In *n*-type photoconductive devices, the gain is defined/interpreted as the number of electrons circulating through the sample per absorbed photons per unit time [14, 15]. The gain can be expressed as the ratio of the hole lifetime to the electron transit time. The annealing has an effect in reducing the surface states, reducing the lifetime enhancement. It also causes an increase in the contact resistance and reduced the voltage drop across the ZnO region. Similar to the GaN case, the present ZnO technology is far from producing low defect-density epitaxial films. ZnO epilayers are known to have a large concentration of dislocations, which result from the low-angle grain boundaries. It has been reported that epitaxial ZnO films grown on sapphire consist of columnar grains slightly twisted along the *c*-axis. A dislocation density of on the order of $1 \times 10^{10} \text{ cm}^{-2}$ order has been reported, which corresponds to the average grain size of $0.1 \mu\text{m}$ [14, 15].

3. Conclusions

The UV detection properties of epitaxial ZnO films grown on sapphire substrates with radio-frequency magnetron sputtering is reported. High responsivity of ZnO photoconductors of 3500 A/W (or a gain of 6000) was obtained at the optical power density of 10^{-7} W/cm^2 , and the value decreases to 1 A/W at 10^{-2} W/cm^2 . The ultra-high responsivity at the low power regime suggested the long lifetime (order of 10 μs) of carriers. The enhanced carrier lifetime was explained by the preferential capture of holes at the recombination centers that exist in the depletion region around grain boundaries and film surface, and the subsequent separation of photogenerated carriers. The strong dependence of the responsivity on the incident power was attributed to the modulation of space charge region width by the photogenerated holes and the resulting change in carrier lifetime [14, 15].

References

- [1] P Meng, S Gu, J Wang, J Hu, J He, "Improving electrical properties of multiple dopant *ZnO varistor* by doping with indium and gallium," *Ceramics International* 44, 1168-1171, (2018).
- [2] C Fei, H Hsu, A Vafanejad, Y Li, Q Zhou, "Ultrahigh frequency *ZnO* silicon lens ultrasonic *transducer* for cell-size microparticle manipulation," *Journal of Alloys and Compounds*, 729, 556-562, (2017).
- [3] B Sarma, BK. Sarma, "Role of residual stress and texture of *ZnO* nanocrystals on electro-optical properties of *ZnO/Ag/ZnO* multilayer *transparent* conductors," *Journal of Alloys and Compounds* 734, 210-219, (2018).
- [4] M Zhang, H Zhang, L Li, K Tuokedaerhan, Z Jia, "Er-enhanced humidity sensing performance in black *ZnO*-based *sensor*," *Journal of Alloys and Compounds* 744, 364-369, (2018).
- [5] Q Sun, Y Men, J Wang, S Chai, Q Song, "Support effect of *Ag/ZnO catalysts* for partial oxidation of methanol," *Inorganic Chemistry Communications* 92, 51-54, (2018).
- [6] J Kim, B Kang, H Jeong, S Kim, S Kang, "Quantum dot light emitting diodes using size-controlled ZnO NPs," *Current Applied Physics* 18, 681-685, (2018).
- [7] S Safa, S Mokhtari, A Khayatian, R Azimirad, "Improving *ultraviolet* photodetection of *ZnO* nanorods by Cr doped *ZnO* encapsulation process," *Optics Communications* 413, 131-135, (2018).
- [8] D You, C Xu, F Qin, Z Zhu, W Liu. "Interface control for pure *ultraviolet* electroluminescence from nano *ZnO* based heterojunction devices," *Science Bulletin* 63, 38-45, (2018).
- [9] S Park, W Hong, J Kim, "Piezoelectric and spontaneous polarization effects on *exciton binding* energy and light emission properties of wurtzite *ZnO/MgO* quantum dots," *Solid State Communications* 261, 21-25, (2017).
- [10] X Liang, L Shen, "Interfacial thermal and electrical transport properties of pristine and nanometer-scale ZnS modified *grain boundary* in *ZnO* polycrystals," *Acta Materialia* 148, 100-109, (2018).
- [11] K Liu, M Sakurai, M Aono, "ZnO based ultraviolet photodetectors," *Sensors* 10, 8604-8634 (2010).
- [12] L Vikas, K Vanaja, P Subha, M Jayaraj, "Fast *UV* sensing properties of n-ZnO nanorods/p-GaN heterojunction," *Sensors and Actuators A: Physical* 242, 116-122, (2016).
- [13] C Pemmaraju, TArcher, R Hanafin, S Sanvito, "Investigation of n-type donor defects in Co-doped ZnO," *Journal of Magnetism and Magnetic Materials* 316, 85-187, (2007).
- [14] Ahmed Nahhas, H Kim, J Blachere, "Epitaxial growth of ZnO films on Si substrates using an epitaxial GaN buffer," *Applied Physics Letters* 78, 1511, (2001).
- [15] Ahmed Nahhas, "Study of ZnO Epitaxial growth and MSM photodetectors," University of Pittsburgh (2001).